Dynamic Configuration of Coactive Micropatterns in the Default Mode Network during Wakefulness and Sleep

Yan Cui[1], Min Li[1], Bharat Biswal[1, 2, *], Wei Jing[1, 3], Changsong Zhou[4], Huixiao Liu[1], Daqing Guo[1, 6, *], Yang Xia[1], Dezhong Yao[1, 5, 6, *]

[1]The Clinical Hospital of Chengdu Brain Science Institute, MOE Key Lab for NeuroInformation, University of Electronic Science and Technology of China, Chengdu 611731, China

[2]Department of Biomedical Engineering, New Jersey Institute of Technology, Newark, NJ 07102, USA

[3]Department of Physiology, School of Basic Medicine and Tongji Medical College, Huazhong University of Science and Technology, Wuhan, China

[4]Department of Physics, Centre for Nonlinear Studies and Beijing-Hong Kong-Singapore Joint Centre for Nonlinear and Complex Systems (Hong Kong), Institute of Computational and Theoretical Studies, Hong Kong Baptist University, Kowloon Tong, Hong Kong

[5]School of Electrical Engineering, Zhengzhou University, Zhengzhou 450001, China

[6]Sichuan Institute for Brain Science and Brain-Inspired Intelligence, Chengdu 611731, China

[*]Corresponding authors: dqguo@uestc.edu.cn, dyao@uestc.edu.cn and bbiswal@gmail.com

Abstract

17

18 The activity in the default mode network (DMN) rapidly fluctuates in different conscious

19 stages during wakefulness and sleep, indicating high complexity for the role of DMN in

20 consciousness. Tracking the dynamics of these fluctuations is critical for deeply understanding

21 the physiological mechanism of consciousness. Here, we propose a coactive micropattern

22 (CAMP) method to extract the dynamic configuration of local field potentials (LFPs) in the

23 rat DMN. Three spatially stable CAMPs were detected from DMN gamma activity (40-80 Hz)

24 across wakefulness and sleep, consisting of a common low-activity level micropattern, an

25 anterior high-activity level micropattern and a posterior high-activity level micropattern.

26 Temporal structures of these CAMPs were specific to different conscious stages. A dynamic

27 balance across CAMPs emerged during wakefulness and was disrupted in sleep stages,

28 demonstrating that the balanced dynamic configuration of CAMPs played a vital role in

29 supporting higher cognitive functions and primary consciousness. Furthermore, all these

30 CAMPs displayed strong phasic relationships to the up-down states of the slow DMN activity

31 during deep sleep. Our study reveals that the consciousness levels of different conscious stages

32 are determined by the dynamic configurations of DMN activity, and provides a potential three-

33 state model for the consciousness during wakefulness and sleep.

34 **Keywords:** default mode network; coactive micropattern; wakefulness and sleep; up-down

35 states; dynamic configuration

1. Introduction

Multimodal imaging studies of the human brain have discovered that several intrinsic connectivity networks (ICNs) co-exist during the resting state(Beckmann et al., 2005; Liu et al., 2017). Dynamic switching within these ICNs displays a hierarchical structure over time for the brain activity at rest and is significantly associated with the cognitive traits(Fox et al., 2016; Vidaurre et al., 2017), suggesting that brain activity is appropriately understood in terms of the dynamic configuration among ICNs. These studies mainly consider each ICN as a whole during brain dynamics but ignore the intrinsic dynamics of individual ICN. Indeed, individual ICN also shows strong fluctuations in brain activity and different ICNs are believed to dominate distinct cognitive functions(Rosazza and Minati, 2011). For a specific brain function, further tracking the dynamic configuration of fluctuations in brain activity at single-ICN level might be critical to reveal the physiological mechanism underlying it.

As a task-negative ICN, the default mode network (DMN) has been highlighted and progressively refined as the key neural correlate of consciousness(Fox et al., 2018; Gusnard et al., 2001; Raichle, 2015; Raichle et al., 2001). DMN connectivity between the frontal and posterior areas is reduced during the slow wave sleep (SWS) stage(Sämann et al., 2011), which displayed low level of consciousness. However, at sleep onset and throughout the rapid eye movement sleep (REM) stage with primary consciousness(Hobson, 2009), the DMN regions persisted in their couplings(Horovitz et al., 2008; Larson-Prior et al., 2009). These findings illustrate that DMN activity is functionally reorganized during sleep and might further reflect levels of consciousness. Additionally, fast and ever-changing dynamics of DMN activity have also been observed in various consciousness levels, and the temporal aspects of spontaneous DMN activity might be associated with conscious processes(Kapogiannis et al., 2014; Panda

3

59 et al., 2016). Therefore, the close association between DMN activity and consciousness

60 represents an important topic to study for an understanding of the physiological mechanism of

61 consciousness by revealing the dynamic configuration of fast DMN activity, which has not

62 been completely elucidated.

63   On the other hand, recent neurophysiological studies identified the up-down state as a

64 biomarker of low-level consciousness, particularly in the deep sleep stage and anesthesia. The

65 up-down state refers to the alternate epochs in which neurons in various brain regions increase

66 and decrease their firing rates in a highly synchronized and stepwise manner at a rate of

67 approximately 0.5–2 Hz(Amzica and Steriade, 1995; Petersen et al., 2003). Moreover, this up-

68 down state emerges in both neuron membrane potentials and local field potentials

69 (LFPs)(Holcman and Tsodyks, 2006), and characterizes the dynamics of slow oscillations

70 during deep sleep(Ji and Wilson, 2007; Lőrincz et al., 2015). However, researchers are still

71 debating the existence of a physiological relationship between the up-down state and the DMN

72 dynamics, another issue that deserves further exploration.

73   In the present study, we developed and applied a new dynamic activity pattern method to

74 address these challenges. The proposed method extracted the dynamic configuration of fast

75 neural activity in different conscious stages based on the coactive phenomena in envelope

76 activity from multi-channels physiological signals. The new method-the coactive micropattern

77 analysis (CAMP)-decomposed the dynamics of neural activity into several instinct CAMPs

78 and defined the configurations across time through the constitutions and transitions among

79 these CAMPs. We then applied the CAMP analysis to the recorded LFPs from rat DMN during

80 wakefulness and sleep. Our results demonstrated the reorganized dynamic configurations of

81 CAMPs for the fast DMN activity in different conscious stages, implying that the dynamic

4

82   configurations of DMN micropatterns might provide underlying neural correlates for the

83   consciousness levels observed during wakefulness and sleep.

84   **2. Material and Methods**

85   **2.1. Dataset.** Twenty-nine male Sprague-Dawley rats were used in our experiment. Firstly,

86   fifteen electrodes, including seven epidural cortical electrodes and eight depth electrodes, were

87   implanted into the brain of each rat under deep anesthesia (sodium pentobarbital, 60 mg/kg

88   body weight, i.p.) at the coordinates proposed by Lu(Lu et al., 2012) (Fig. 1, Table 1). The

89   reference electrode was placed in the cerebellum, and two electromyographic (EMG)

90   electrodes were implanted bilaterally in the dorsal neck muscles. Here the cerebellum was

91   chosen for the placement of the reference electrode, for that there was lower neural activity in

92   the cerebellum and the cerebellum was not involved in many cognitive functions. Notably, 0.6

93   ml of atropine sulfate (0.5 mg/ml, s.c.) was injected during electrode implantation to prevent

94   excess secretions from the respiratory tract. Meanwhile, the body temperature of the rats was

95   maintained at 37 degrees centigrade with a heating pad. Then, all electrodes were welded to

96   connectors and fixed on the skull of the rat with dental acrylic. After the surgical procedure,

	A-P	M-L	D-V
PrL	4.2	± 0.8	3
OFC	3.7	± 1.8	4.7
CG	1.7	± 0.7	2.6
RSC	-3.3	0	0
HIP	-4.3	± 1.4	3
PPC	-4.5	± 4	0
V2	-5.2	± 2.4	0
TE	-5.2	± 8	5

97   **Table 1.** Coordinates of the 15 electrodes (mm). A-P, M-L, and D-V indicate anterior-posterior, medial-

98   lateral, and dorsal-ventral directions, respectively. PrL, prelimbic cortex; OFC, orbital cortex; CG,

99   cingulate cortex; RSC, retrosplenial cortex; HIP, hippocampus; PPC, posterior parietal cortex; V2,

100   secondary visual cortex; TE, temporal association cortex.
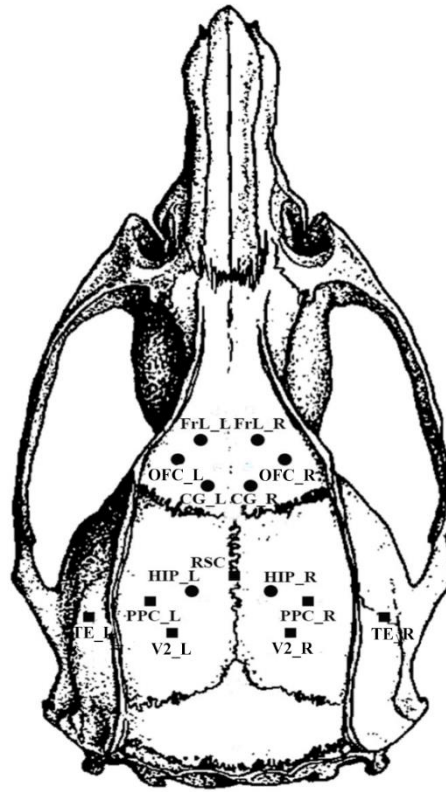
■ **epidural electrode** ● **depth electrode**

Fig. 1. The placement of 15 intracranial electrodes.

penicillin G was administered to prevent infection, and all rats were allowed at least 2 weeks

for recovery before the recording session started. All experimental animal procedures were

approved by the Institutional Animal Care and Use Committee of the University of Electronic

Science and Technology of China.

Prior to the recording sessions, the rats were habituated to the experimental environment

and the recording cable for 2 days. During the recording session, all rats were placed in a glass

box on a 12-h light/dark cycle (lights on at 8:00 am). Each recording electrode was connected

to an acquisition system (Chengyi, RM62160, China). Electrophysiological signals (LFPs) and

videos were synchronously and continuously acquired for 72 h. The amplified and filtered

(0.16–100 Hz for LFPs, 8.3–500 Hz for electromyogram (EMG), and 50-Hz notch filter)

signals were stored on a hard disk (Lenovo Company, USA), and the sample frequency was

114   set to 1,000 Hz. All experiments were performed in a noise-attenuated room, where the

115   background noise was set to 32.2 ± 3.0 dB and the temperature was maintained at 25 ± 0.5

116   degrees centigrade. The experimenter entered the noise-attenuated room to replace food and

117   water and clean cages at 12:00 am daily.

118   The dataset used in the current study was selected from the last 24 h of the total recording

119   and was separated into three stages, including the resting (AWAKE), slow wave sleep (SWS)

120   and rapid eye movement (REM) sleep stages. The rules for selecting each stage were based on

121   LFP, EMG and videos, which have been summarized in our previous publications(Jing et al.,

122   2017). Briefly, the scoring of the awake and sleep stages were performed by several experts.

123   We included 29 rats in the current study. For each rat, 30 segments in different stages were

124   recorded, and each segment lasted 10 s (a total of 300 s of LFPs).

125   **2.2. The coactive micropattern (CAMP) algorithm.** Using functional magnetic resonance

126   imaging (fMRI) data, Liu and colleagues(Liu et al., 2013; Liu and Duyn, 2013) used the

127   coactive pattern method, a point process approach, to identify a set of CAPs with relevant

128   network features to resting state networks, including the default mode network (DMN). In the

129   present study, we developed a coactive micropattern (CAMP) measurement and specifically

130   employed it to analyze neurophysiological data. An overview and procedure of the CAMP

131   method is shown in Fig. 2. This method was used to extract CAMPs based on the extreme

132   values of envelope signals at a high temporal resolution and reveal the fast dynamics of

133   multichannel LFPs.

134   Several steps were involved in the CAMP method. First, the original data were bandpass

135   filtered into specific frequency bands. In our study, we filtered the original LFPs into the

136   gamma (40-80 Hz) frequency band for the neural correlation between DMN gamma oscillation

7
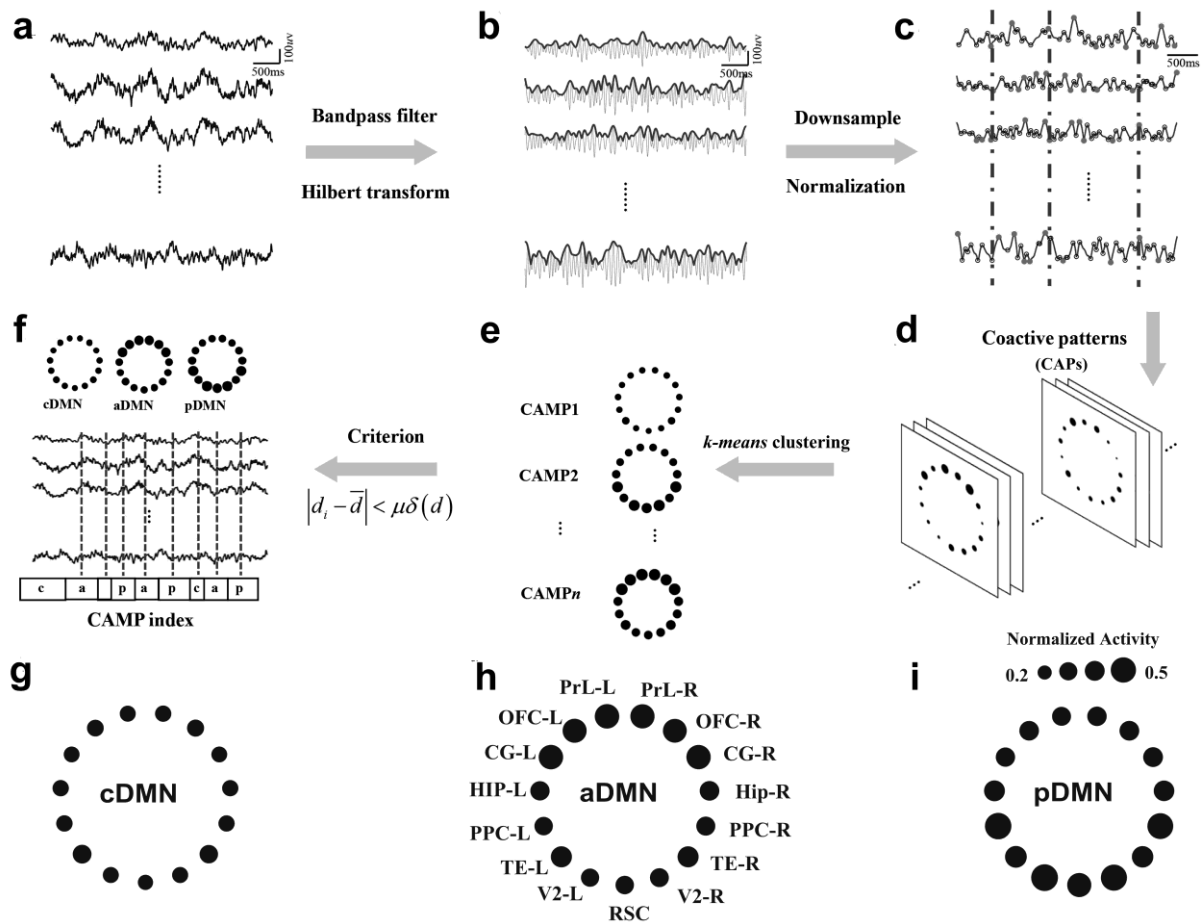
Fig. 2. Schematic of the CAMP procedure and three CAMPs of gamma activity in the DMN during wakefulness and sleep. (a) The original LFPs. (b) The envelope signals (blue lines) were extracted by applying the Hilbert transform to the bandpass-filtered signals (gray lines). (c) All the envelope signals were downsampled (blue lines), and the extreme values were detected as the active points for each channel (red dots). The dotted lines suggest the coactive points in which more than N (N=7 in the present study) active points were observed across DMN regions. (d) The coactive patterns were the maps of activity of all DMN regions at coactive points. (e) The k-means clustering algorithm was applied to all coactive patterns to detect the CAMPs. (f) A criterion was employed to remove several coactive points and increase the aggregation of the CAMPs. The final CAMPs and CAMP index detected in this step were subjected to further analyses. (g) Spatial structure of the common low-activity level micropattern (cDMN). (h) Spatial structure of the anterior high-activity level micropattern (aDMN). (i) Spatial structure of the posterior high-activity level micropattern (pDMN).

with the cognitive functions. Second, the Hilbert transform was applied to the filtered data to

152   obtain the envelope signals (Fig. 2b). These envelope signals were normalized and

153   downsampled (from 1,000 Hz to 100 Hz) to improve the signal-to-noise ratio (SNR) (Fig. 2c).

154   The envelope signals were normalized by restricting the maximum value of the normalized

155   envelope signal to 0.9 and the minimum value to 0.1. Third, the active points for each channel

156   of envelope signals were then defined as the extreme points of the envelope signals, including

157   local maximum and minimum values. Afterwards, the coactive patterns (CAPs) of the brain

158   were introduced from normalized and down-sampled envelope signals for all states. The CAPs

159   were the brain maps in which more than one brain region displayed active points at the same

160   time point (Fig. 2d), and totally there were 1724646 CAPs that were extracted. Thus, we

161   considered the number of brain regions with active points at the same time (parameter N) as

162   one important parameter for extracting these coactive patterns.

163   After extracting the CAPs from envelope signals, we employed the k-means clustering

164   algorithm to all the CAPs based on their spatial similarity to decompose the CAMPs (Fig. 2e).

165   By clustering the CAPs into several distinct groups, we temporally divided the brain activity

166   into multiple CAMPs. We repeated the k-means clustering with $k = 2, ..., 10$ and applied the

167   contour coefficient estimation (i.e., the sum of the squared errors, SSE) to determine the

168   optimal number of distinct groups and select the optimal number of CAMPs. The optimal

169   number of CAMPs was 3 in our study, according to the elbow of the curve between the k

170   values and SSE values (Supplementary Fig. 1b).

171   Next, the CAMPs were fit back to the coactive patterns (CAPs), assigning each CAP to

172   the CAMP class with the lowest squared Euclidean distance to the three CAMPs. The CAMP

173   index was then obtained from the assignment, which showed the temporal sequence of CAMPs

174   in the gamma activity of the DMN. Then, we carefully updated the CAMPs and CAMP index

175   according to the CAPs that belong to the same CAMP class using the following criterion:

176     $\left| d_i - \overline{d} \right| < \mu \delta(d)$, where d_i is the squared Euclidean distance between the i th coactive

177   pattern with its assigned CAMP, $\overline{d}$ is the mean of all distance, $\delta(d)$ is the standard

178   deviation of these distance, and μ is the penalty parameter we determined. If the distance

179   did not conform to this criterion, then we removed the assignment of the corresponding CAPs

180   from any CAMP class (Fig. 2f). Afterwards, we applied the k-means clustering algorithm to

181   all remaining original CAPs using the same k value detected previously and redefined the

182   clusters. This step was iterated until all distances obeyed this criterion. Using this criterion,

183   we precisely determined the final spatial structures of CAMPs and the CAMP index. Notably,

184   if the CAP was not assigned to any CAMP, we removed it from the CAMP index. 261344

185   CAPs were removed based on this criterion and there were 1463303 CAPs used in subsequent

186   analysis. The final CAMP index only contained the assignments of all CAPs to their

187   corresponding CAMPs.

188   In the present study, we calculated the number of CAPs for different N values ranging

189   from 2 to 15 (Supplementary Fig. 1a) and decomposed the CAMPs from these CAPs. Under

190   different N values, the derived CAMPs exhibited similar spatial structures (Supplementary

191   Fig. 2). Therefore, considering the complexity of the calculation and requirement for

192   additional information about DMN dynamics, we finally set N to 7 in the current study.

193   Additionally, we also altered the penalty parameter μ from 1.5 to 3 (step size of 0.1) and

194   described how the proportion of removed CAPs varied with different μ values

195   (Supplementary Fig 1c). By extracting the CAMPs with different μ values, we observed

196   similar spatial structures of these CAMPs, implying that the penalty parameter might not affect

197   the CAMPs (Supplementary Fig. 3). Therefore, we finally set the value of this parameter to 2

198 in the subsequent analysis.

199 All our analyses of the CAMP algorithm were performed using our own custom MATLAB

200 (release 2019a) scripts and the scripts for CAMP algorithm are available in the Mendeley

201 website (https://data.mendeley.com/datasets/p522rj449p/draft?a=0ef3b254-520e-456e-b257-

202 c398ef632148). If a special description was not included, we extracted the CAMPs of all the

203 CAPs from whole segments acquired from rats in all three conscious stages. For every segment,

204 the CAMPs were obtained by averaging the CAPs belonging to their corresponding clusters

205 in that segment. Meanwhile, the CAMP index of each segment was also acquired from the

206 total CAMP index.

207 **2.3. Estimation of the CAMP features.** In the present study, we employed five measurements

208 to characterize the features of CAMPs and the CAMP index of each segment.

209 The total occurrence represented the number of CAPs assigned to each CAMP, and the

210 occurrence probability was the proportion of the total occurrence of the number of all CAPs.

211 The total duration characterized the entire time required for each CAMP and the duration

212 probability represented the proportion of that.

213 The duration of one CAP was defined as follows: the start time was the mid-point between

214 the time point of this CAP and the preceding CAP, and the end time was the mid-point between

215 the time point of this CAP and the next CAP.

216 We first defined the event for each CAMP to determine the mean duration of each CAMP.

217 An event for each CAMP was that the coactive pattern before or after it should be different

218 from itself. Thus, in the CAMP index, if the neighboring CAPs belonged to the same CAMP,

219 then they should be included in one event for that CAMP. Using this approach, we obtained a

220 new CAMP index in which the neighboring coactive patterns did not belong to the same

11

221   CAMP. We separately estimated the numbers of events for all CAMPs, and the mean duration

222   for each CAMP was calculated by dividing the total duration by the number of events for that

223   CAMP.

224   All values of these CAMP features were calculated for each segment (10 s). The values

225   of these features were averaged based on the rat and conscious stage to which they belonged

226   to calculate the values of CAMP features for each rat in different conscious stages.

227   **2.4. Transition probabilities (TPs) for pairs of CAMPs.** The transition probabilities for pairs

228   of CAMPs were the one-step and direct transitions among them. These TPs were separately

229   estimated from the new CAMP index for each segment. Six types of direct transitions were

230   identified in the new CAMP index. The TP for one direct transition was calculated by dividing

231   the number of this transition by the total number of all direct transitions.

232   **2.5. Reliability test for the three CAMPs across the 29 rats and different conscious stages.**

233   We initially applied the CAMP analysis to the segments obtained from each rat in the AWAKE,

234   SWS and REM sleep stages to assess the reliability of these CAMPs. Three different CAMPs

235   were identified for each for each rat in each conscious stage (29*3*3 total CAMPs).

236   The reliability of CAMPs across rats was determined by estimating the correlation

237   coefficients of the CAMPs among pairs of rats in the same conscious stage using the Pearson

238   correlation method. These correlation coefficients were then averaged to obtain the reliability

239   of each CAMP in each conscious stage (3*3). For different conscious stages, we next averaged

240   the correlations across CAMPs and obtained the reliabilities of all CAMPs for each stage.

241   For the analysis of the reliability of CAMPs across different conscious stages, we first

242   estimated the correlation coefficients of CAMPs among pairs of conscious stages for each rat

243   (29*3*3). Then, the whole correlation coefficient was averaged and the reliability of CAMPs

244   across stages was obtained (3*3).

245   **2.6. Randomization test for the CAMP index**. The randomization tests were applied to the

246   new CAMP indices in the AWAKE, SWS and REM sleep stages(Lehmann et al., 2005). The

247   null hypothesis was that if the transition from a preceding CAMP to the next CAMP occurred

248   randomly, then the observed TPs would depend on the occurrence probability of CAMPs.

249   During the test, we considered the expected TP from CAMP X to CAMP Y to be

250 $$P_{X \to Y}^* = P_X P_Y / (1 - P_X), \qquad (1)$$

251   where $P_X (P_Y)$ is the occurrence probability for CAMP $X(Y)$. The difference between the

252   expected TP and the observed TP was then assessed by calculating the chi-square distance

253 $$\sum_{X,Y} \left(P_{X \to Y} - P_{X \to Y}^* \right)^2 / P_{X \to Y}^*, \qquad (2)$$

254   where the sum was calculated for all 6 pairs of CAMPs for which $X \neq Y$. The randomization

255   test (permutation test) was then performed to statistically analyze the significance of this

256   distance between the observed TP and expected TP. The permutation test was performed by

257   shuffling the order of coactive patterns. The number of randomizations in the permutation test

258   was set to 10,000 in our study, and the probability was determined by the rank of the observed

259   difference among the randomly obtained differences.

260   **2.7. Phasic relationships between CAMPs and up-down states in the slow oscillations of**

261   **the DMN during deep sleep.** We first averaged the DMN activity to obtain the activity of

262   anterior DMN and posterior DMN in the SWS stage and to assess the phasic relationship

263   between CAMPs and up-down states. The average activity was then bandpass-filtered at 0.5-

264   2 Hz and downsampled from 1,000 Hz to 100 Hz, which coincided with the CAMP algorithm.

265   Using this approach, we finally obtained the downsampled slow oscillations in the anterior

266   DMN and posterior DMN regions. Then, the Hilbert transform was applied to these slow

267   oscillations to obtain the instantaneous phase for both slow activity in the anterior DMN and

268   posterior DMN activity. By combining the acquired instantaneous phase and timing of each

269   CAMP, we obtained the instantaneous phases of all CAMPs in the slow activity of the anterior

270   DMN and posterior DMN, and the distributions of phases for the cDMN, aDMN and pDMN

271   in the SWS stage. Finally, we employed the Rayleigh test to analyze the non-uniformity of

272   these distributions of phases for the three CAMPs.

273   **2.8. Statistical analysis.** The statistical comparisons of the CAMP features and the TPs among

274   CAMPs across the three stages were performed using the methods described below. First, an

275   ANOVA was performed among all three stages, and then Student's t test was performed as the

276   post hoc test to determine the significance of differences between pairs of stages. In addition,

277   the p values derived from Student's t tests were corrected with the false discovery rate (FDR)

278   correction.

279   **3. Results**

280   **3.1. Three CAMPs of gamma activity in the DMN during wakefulness and sleep.** The

281   CAMP analysis procedure developed in the present study is schematically illustrated in Fig. 2

282   and section 2.2. The concatenated gamma activity in the DMN of all rats and all stages during

283   wakefulness and sleep was decomposed into three distinct CAMPs, including a common low-

284   activity level micropattern (cDMN), an anterior high-activity level micropattern (aDMN) and

285   a posterior high-activity level micropattern (pDMN). In the cDMN, all DMN regions showed

286   similar and low levels of activity (mean normalized activity: 0.2577 ± 0.0041, Fig. 2g),

287   indicating a potential cooperation of these regions in this type of CAMP. However, two

288   different levels of activity were observed in both the aDMN and pDMN. The aDMN exhibited

289   relatively higher levels of activity in the anterior DMN regions (i.e., the prelimbic cortex (PrL),

14

	cDMN	aDMN	pDMN	Mean Reliability
AWAKE	0.5806	0.8043	0.8504	0.7451
SWS	0.7588	0.6472	0.8544	0.7535
REM	0.4257	0.6951	0.8843	0.6684

Table 2. The reliabilities (correlation coefficients) of CAMPs in the three stages across rats.

|	AWAKE *vs.* SWS	AWAKE *vs.* REM	SWS *vs.* REM	Mean Reliability
cDMN	0.7214	0.6352	0.5122	0.6229
aDMN	0.7910	0.8650	0.7087	0.7882
pDMN	0.8406	0.9091	0.8302	0.8600

Table 3. The reliabilities (correlation coefficients) of CAMPs across the three conscious stages.

the orbitofrontal cortex (OFC) and the cingulate gyrus (CG), mean normalized activity: 0.3868 ± 0.0018) and lower activity in the posterior DMN structures (i.e., the hippocampus (HIP), the posterior parietal cortex (PPC), the visual cortex area (V2) and the retrosplenial cortex (RSC), mean normalized activity: 0.3050 ± 0.0060, Fig. 2h). In the pDMN, the posterior DMN structures displayed higher levels of activity (mean normalized activity: 0.3793 ± 0.0145), while the anterior DMN regions showed relatively lower levels of activity (mean normalized activity: 0.3073 ± 0.0021, Fig. 2i). Accordingly, both the aDMN and pDMN were considered the high-activity micropatterns in DMN dynamics.

We separately decomposed the CAMPs for each rat in every conscious stage and tested their reliability across all 29 rats and different conscious stages by calculating the Pearson correlation coefficient to assess the spatial stability of these detected CAMPs. All three CAMPs exhibited high stability with large correlation coefficients among different rats during wakefulness and sleep (mean correlation coefficients: r = 0.7451, r = 0.7535, r = 0.6684 for the AWAKE stage, SWS stage and REM sleep stage, respectively; Table 2). Besides, the spatial structures of these CAMPs were also similar in distinct conscious stages (mean correlation coefficients: r = 0.6229, r = 0.7882, r = 0.8600 for AWAKE stage, SWS stage and REM sleep
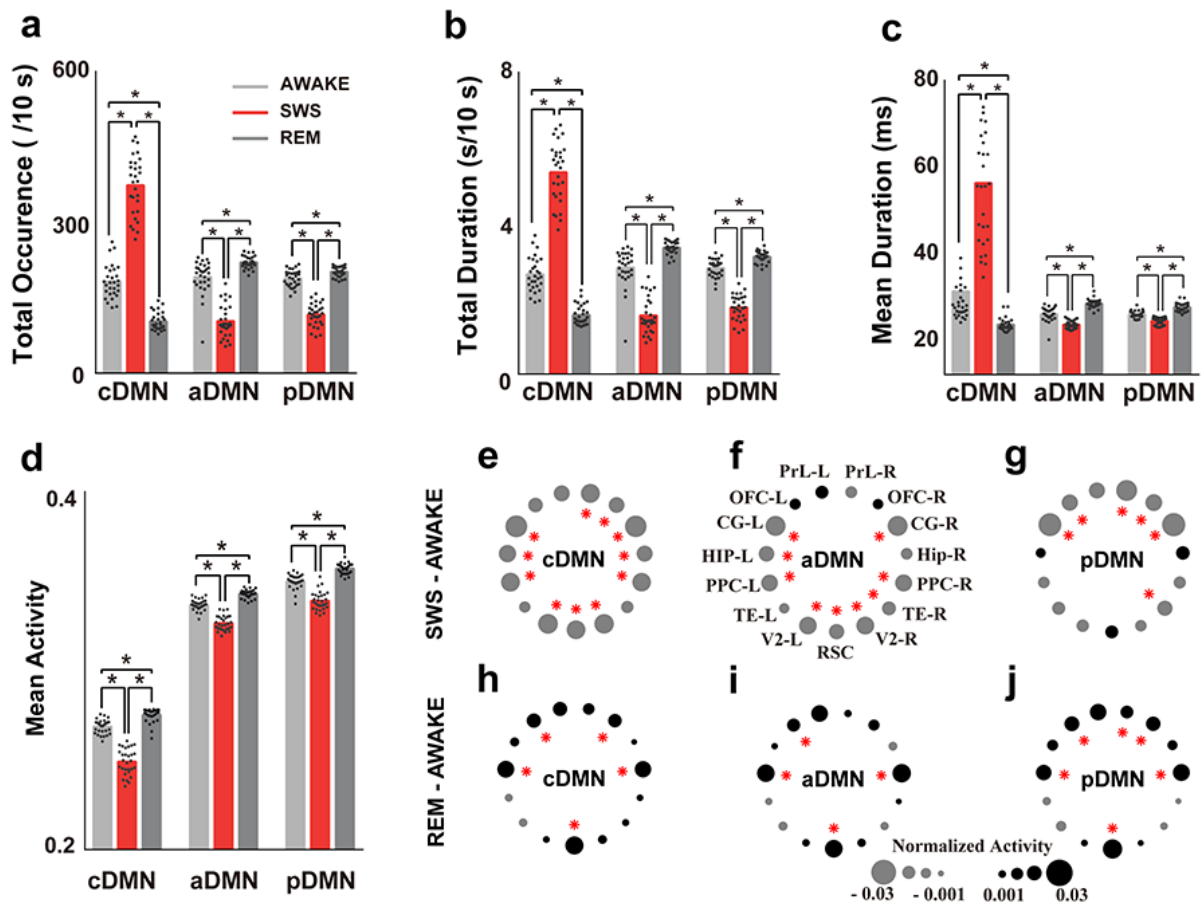
Fig. 3. Comparisons of the temporal features and activity levels of each CAMP during wakefulness and sleep. (a) Comparisons of the total occurrence of each CAMP in different conscious stages. The dots represent the values obtained from 29 rats, and the black stars indicate significant differences with a corrected p<0.001. (b) Comparisons of the total duration. (c) Comparisons of the mean duration. (d) Comparisons of the mean DMN activity during wakefulness and sleep for different CAMPs. (e-j) Comparisons of activity in DMN nodes for different CAMPs across different conscious stages: (e and h) cDMN, (f and i) aDMN, and (g and j) pDMN. Gray dots indicate decreased normalized activity and black dots indicate increased normalized activity. The size of the dot reflects the value of the difference, and the red stars indicate significance differences with a corrected p<0.001.

stage, respectively; Table 3). These findings demonstrated high reliability and robustness of these CAMPs.

3.2. The temporal features and activity levels of each CAMP during wakefulness and sleep. We computed several temporal measurements to characterize the features and dynamics

324   of these CAMPS during wakefulness and sleep, including the total occurrence (occurrence

325   probability), the total duration (duration probability) and the mean duration. All these features

326   represented the temporal properties of these CAMPs in different conscious stages. Based on

327   the comparisons, all features of the low-activity micropattern cDMN displayed the largest

328   values in the SWS stage and the smallest values in the REM sleep stage, and the two high-

329   activity micropatterns (i.e., the aDMN and pDMN) exhibited the largest values for all features

330   in the REM sleep stage and the smallest values in the SWS stage (Fig. 3a-3c). These opposite

331   alterations in features between low-activity micropatterns and high-activity micropatterns

332   above-mentioned comparisons were also highly significant, implying that the alterations in the

333   suggested that these two types of CAMPs observed in DMN dynamics might represent

334   different physiological characteristics of consciousness during wakefulness and sleep. The

335   CAMP features in different conscious stages were remarkable and would help improve our

336   knowledge of the changes in consciousness during wakefulness and sleep.

337   However, all of these CAMPs displayed different activities in DMN regions during

338   wakefulness and sleep. In particular, all DMN regions exhibited reduced activity during SWS

339   stages in all CAMPs (Fig. 3e-3g). Moreover, the regions with significantly reduced activity in

340   the aDMN were the posterior DMN structures, and the regions with significantly reduced

341   activity in the pDMN were the anterior DMN regions, which all showed relatively lower

342   activity in the AWAKE stage. The significant decrease in the activity of regions with a lower

343   level activity indicated a preservation of the major activity in high-activity micropatterns in

344   deep sleep (Fig. 3f-3g, red stars). However, all CAMPs displayed increased activity in most

345   DMN regions during the REM sleep stage. The activity in the HIP, OFC and RSC regions was

346   significantly increased during the REM sleep stage in all CAMPs, implying the importance of
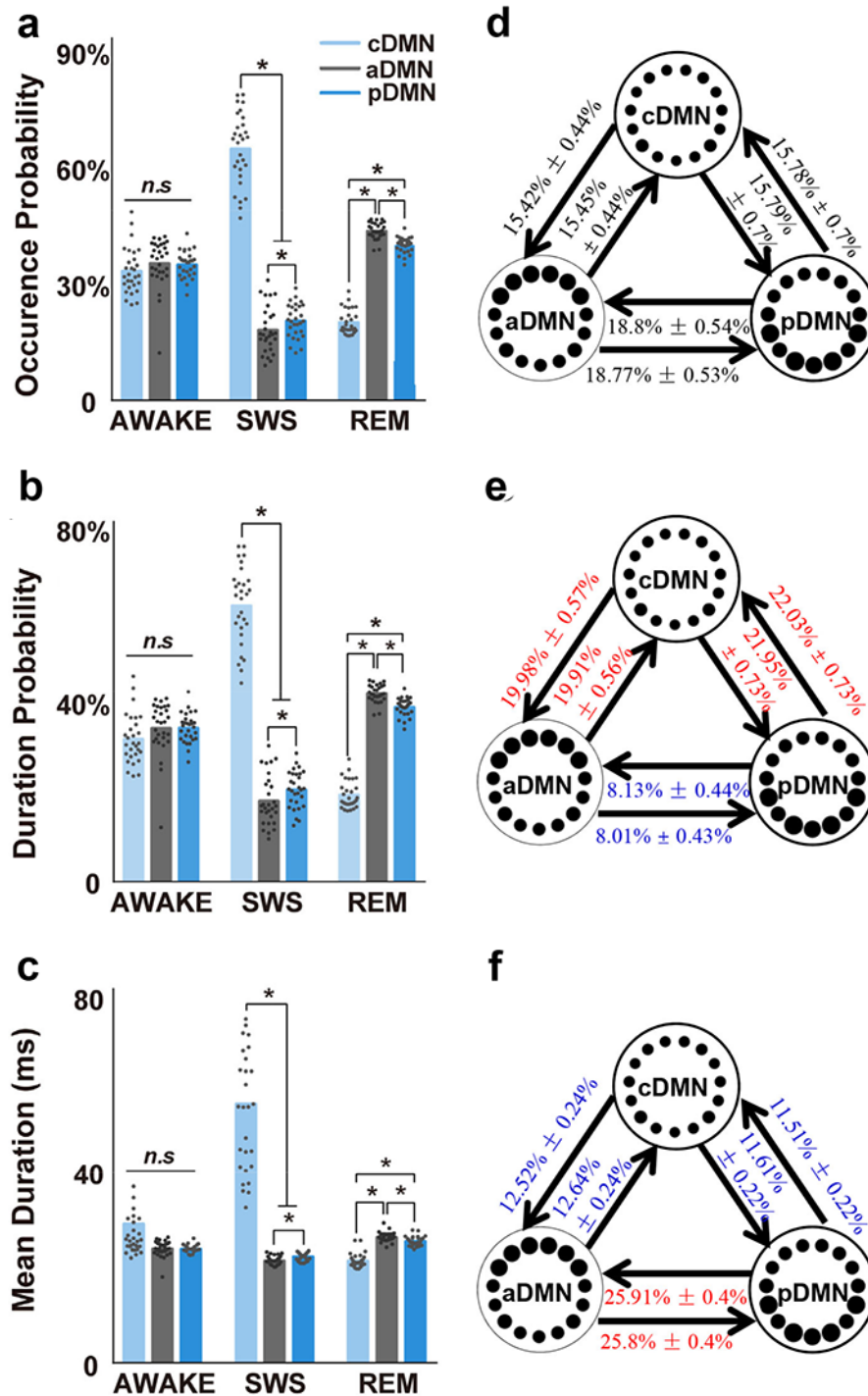
Fig. 4. Characteristics of CAMPs and the transitions among them in different stages of consciousness during wakefulness and sleep. (a) Comparisons of the occurrence probability for all CAMPs in the three stages. The black dots indicate the values of the occurrence probability obtained from 29 rats in different CAMPs and stages. The black stars indicate significant differences with a corrected p<0.001. (b) Comparisons of the duration probability. (c) Comparisons of the mean duration. (d-f) The transition structures among CAMPs for the AWAKE (d), SWS (e) and REM sleep stages (f). All the numbers indicate the mean TPs calculated for the 29 rats and the standard deviation. The numbers in blue

355   indicate a significantly lower transition probability than observed in the AWAKE stage, and the

356   numbers in red indicate a significantly higher transition probability. The significance level is a

357   corrected p<0.001.

358

359   these DMN regions for REM sleep (Fig. 3h-3j, red stars). In addition, the mean activity level

360   of each CAMP exhibited a similar variation trend across different conscious stages. The lowest

361   mean activity of CAMPs was observed in the SWS stage, while the highest mean activity was

362   observed in the REM sleep stage (Fig. 3d).

363   **3.3. The constitutions and transitions of CAMPs during wakefulness and sleep.** The

364   configurations of these CAMPs involved in DMN dynamics in different conscious stages were

365   also distinct (Fig. 4a-4c). All CAMPs presented similar features in the AWAKE stage

366   (occurrence probability: 32.12%, 34.12% and 33.75%; duration probability: 31.68%, 34.15%

367   and 34.17%; and mean duration: 29.79 ms, 24.41 ms and 24.37 ms for the cDMN, aDMN and

368   pDMN, respectively. No significant differences in all features were observed.), indicating that

369   their roles were equivalent and a dynamic balance in DMN activity might exist among CAMPs

370   at wakeful rest. However, the cDMN became the dominant activity pattern of DMN dynamics

371   in the SWS stage, as indicated by its largest occurrence probability (62.66%, 17.56% and 19.78%

372   for the cDMN, aDMN and pDMN, respectively), duration probability (61.47%, 18.02% and

373   20.51% for the cDMN, aDMN and pDMN, respectively) and mean duration (55.58 ms, 21.89

374   ms and 22.78 ms for the cDMN, aDMN and pDMN, respectively) among all CAMPs. The

375   predominant constituent of the low-activity micropattern suggested that all the DMN regions

376   might be in a state of low activity and that the DMN activity preferred a silent pattern in deep

377   sleep. Unlike the SWS stage, the two high-activity micropatterns were the main CAMPs

378   observed in the REM sleep stage, as indicated by the remarkably larger values for all features

19

379 of the aDMN and pDMN than the cDMN (occurrence probability: 19.42%, 42.05% and

380 38.53%; duration probability: 19.33%, 41.84% and 38.83%; and mean duration: 21.88 ms,

381 26.92 ms and 26.01 ms for the cDMN, aDMN and pDMN, respectively). The greater

382 percentage of high-activity micropatterns during REM sleep suggested a reactivation of DMN

383 activity in this consciousness stage. In addition, in the comparison between the two high-

384 activity micropatterns, the aDMN displayed significantly larger values for the three features,

385 implying a more important role of the aDMN in REM sleep.

386 Meanwhile, the temporal concatenations of these CAMPs (i.e., the CAMP indices) in

387 different consciousness stages also showed specific changes. We first performed a

388 randomization test to examine the transition structures of these CAMP indices in different

389 stages. The transitions among CAMPs occurred randomly in the AWAKE stage (p = 0.8157),

390 indicating that the transition probabilities (TPs) of pairs of CAMPs in the resting state were

391 proportional to their occurrences. However, these transitions did not occur randomly in the

392 SWS (p<0.0001) or REM sleep stages (p<0.0001), which suggested the stabilization of the

393 structures of the CAMP indices during the sleep cycle. These stabilizations further implied the

394 existence of several preferred transitions among CAMPs in the SWS and REM sleep stages.

395 Next, we compared the transition probabilities (TPs) for pairs of CAMPs between the two

396 sleep stages and the AWAKE stage. The TPs of different pairs of CAMPs in the AWAKE stages

397 were similar (no significant differences among all TPs, Fig. 4d), suggesting the presence of

398 balanced state transitions among all CAMPs at rest. However, the TPs within the two high-

399 activity micropatterns showed significant reductions in the SWS stage, while the TPs between

400 high-activity micropatterns and the low-activity micropattern increased significantly (Fig. 4e).

401 These changes in TPs emphasized the functional role of inhibitory activity in DMN regions in

20
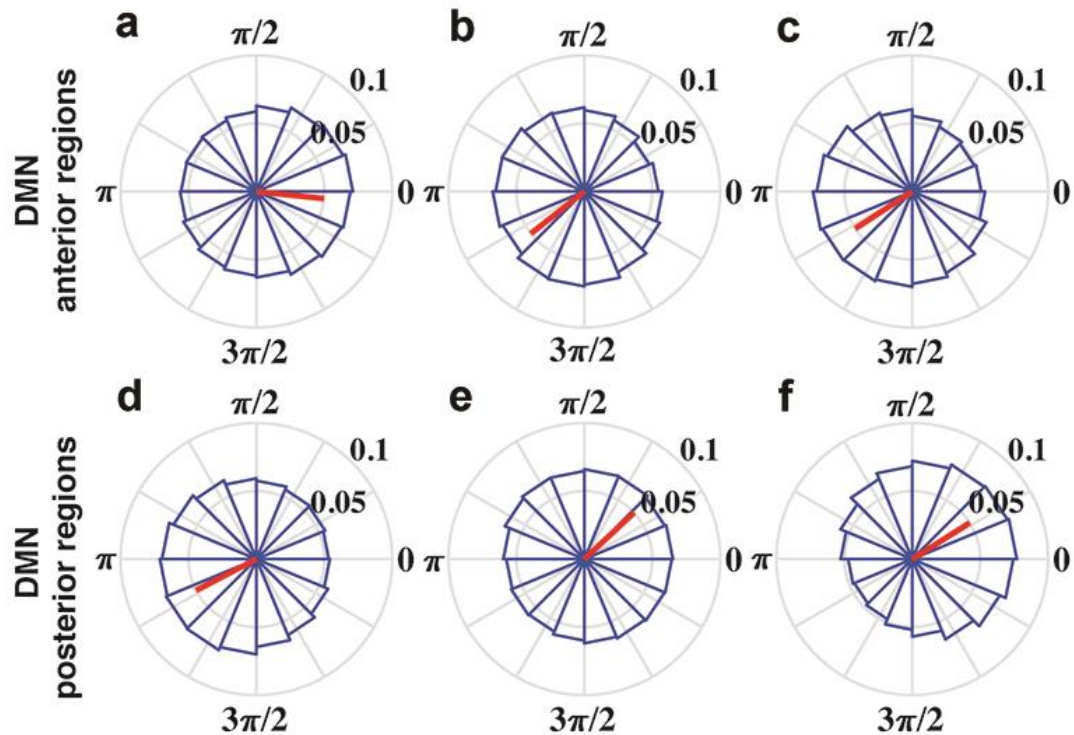
Fig. 5. Phase locking relationship between each CAMP with slow oscillations in the SWS stage. (a-c) The phase locking relationships between the cDMN (a), aDMN (b) and pDMN (c) with the slow oscillations in anterior DMN regions. (d-f) The phase locking relationships between the cDMN (d), aDMN (e) and pDMN (f) with the slow oscillations in posterior DMN regions. The red lines showed the significant directionality with Rayleigh test p<0.001.

deep sleep. On the other hand, the TPs in the REM sleep stage displayed different alterations than in the SWS stage, including significantly increased TPs within high-activity micropatterns and a remarkable decrease in TPs between high-activity micropatterns and the low-activity micropattern (Fig. 4f). The increased transitions within the two high-activity micropatterns revealed increased activation of DMN regions during REM sleep. Based on these findings, the CAMP indices and the functional roles of these CAMPs were specific for different conscious stages. The alterations in DMN activity during wakefulness and sleep might be attributed to the specific temporal combinations of the CAMPs constituting the activity in different conscious stages rather than the spatial structures of CAMPs themselves,

418 which were rather stable across different stages.

419 **3.4. Strong phasic relationships between CAMPs with the up-down states in the SWS**

420 **stage.** Up-down states are considered the predominant pattern of slow oscillations (0.5-2 Hz)

421 during the SWS stage. By estimating the phase distribution of each CAMP in the anterior and

422 posterior DMN slow activity with the Hilbert transform, we observed that these CAMPs

423 displayed strong phasic relationships with the up-down states in the SWS stage. The cDMN

424 preferred the down state of anterior DMN activity (Fig. 5a, significant directionality: 1.97π,

425 red line) and the up state of posterior DMN activity (Fig. 5d, significant directionality: 1.16π,

426 red line). Additionally, both the aDMN and pDMN were phase locked to the up state of anterior

427 DMN activity (Fig. 5b, significant directionality: 1.21π for aDMN. Fig. 5c, significant

428 directionality: 1.18π for pDMN) and the down state of posterior DMN activity (Fig. 5e,

429 significant directionality: 0.23π for aDMN. Fig. 5f, significant directionality: $0.18\ \pi$ for

430 pDMN) , implying that these two high-activity micropatterns might belong to the same activity

431 pattern of slow oscillations of the DMN in deep sleep. Furthermore, the difference of

432 significant directionality of all CAMPs suggested that the slow oscillations in anterior and

433 posterior DMN regions tended to have a phasic shift about π during deep sleep. Accordingly,

434 our proposed CAMPs could also reflect the up-down states of DMN slow activity in the SWS

435 stage and there existed a close physiological association between the up-down states with

436 DMN dynamics.

437 **4. Discussion**

438 In the present study, we developed a CAMP algorithm and applied it to reveal the

439 dynamics of gamma activity in rat DMN during wakefulness and sleep. Our results indicated

440 that the fast dynamics of gamma activity in the DMN were decomposed into three different

441 CAMPs (i.e., micropatterns) in different conscious stages, including the cDMN, aDMN and

442 pDMN. These CAMPs showed stable spatial structures across wakefulness and sleep, while

443 their dynamic configurations were specific to different conscious stages. In addition, all these

444 CAMPs were strongly phase locked to the up-down states in the SWS stage, suggesting the

445 temporal sequence of the neural relationship between up-down states and DMN dynamics.

446 Our findings described the distinct dynamic configurations of gamma activity in the DMN

447 during wakefulness and sleep, and proposed a three-state model to reveal the fundamental

448 neural mechanism by which DMN dynamics mediate consciousness.

449 **4.1. Physiological significance of three CAMPs.** Previous studies have reported a strong

450 correlation between electrophysiological gamma activity and blood oxygen level-dependent

451 (BOLD) signals(Logothetis, 2002; Logothetis et al., 2001; Magri et al., 2012; Scheering et al.,

452 2016). Besides, DMN regions also show deactivation in the gamma frequency during the

453 performance of external tasks in several EEG studies(Karim Jerbi*† et al., 2010; Ossandon et

454 al., 2011), indicating the importance of gamma oscillation in DMN activity. Hence, we

455 specifically focused on the fast dynamics of gamma activity in the DMN in the current study.

456 The gamma activity in the rat DMN was decomposed into three stable CAMPs during

457 wakefulness and sleep that exhibited distinct spatial structures. The differences in these

458 CAMPs provided direct electrophysiological evidence that the DMN regions might not be

459 activated simultaneously. Moreover, all these CAMPs lasted for approximately forty

460 milliseconds, and different CAMPs had distinct periods. These phenomena exhibited

461 differences in the activation times of anterior and posterior DMN structures in the fast

462 dynamics and further illustrated the diversity in the latencies for both the excitation and

463 inhibition of DMN regions(Brett L. Foster, Mohammad Dastjerdi, 2012; Foster et al., 2015).

464   Indeed, functional and neuroanatomical studies have separated the structure of the DMN

465   into a parietal subnetwork and a prefrontal subnetwork in both human and animal brains(Cui

466   et al., 2018; Hagmann et al., 2008; Lu et al., 2012; Wu et al., 2017). In the present study, we

467   not only reinforced this finding from the aspect of fast DMN dynamics but also provided a

468   possible dynamic substrate for this separation of the DMN structure. As a key component of

469   the DMN, the prefrontal cortex has historically been posited to integrate interoceptive and

470   exteroceptive information from multisensory stimuli for processing information about the

471   internal and external milieu of the body(Ongur and Price, 2000). Accordingly, we speculated

472   that the high-activity micropattern aDMN might be a type of DMN pattern that makes

473   inferences and guides actions in a timely and environmentally relevant manner.

474   Meanwhile, the retrosplenial cortex (RSC) located in the parietal DMN, another key area

475   in the DMN, has extensive connections and is topographically organized with the hippocampal

476   formation. The projections between the RSC and hippocampal formation provide an important

477   pathway regulating learning, memory and emotional behavior(Wyss and Vangroen, 1992).

478   Furthermore, the hippocampal formation is a limbic structure that forms direct or indirect

479   connections to the other DMN regions. Therefore, the high-activity micropattern pDMN

480   detected in the present study might be a type of DMN activity pattern associated with memory

481   and emotional behavior. Additionally, both the aDMN and pDMN were strongly phase locked

482   to the up state of anterior DMN activity and the down state of posterior DMN activity during

483   the SWS stage, indicating that they may reflect similar performance for the up-down states of

484   slow oscillations during DMN dynamics. Moreover, these two high-activity micropatterns

485   together accounted for more than 70% of the time in the resting state, which helps to explain

486   why the brain requires a high basal cerebral blood flow and metabolism for spontaneous

487   activity(Raichle and Mintun, 2006).

488   In addition, we observed a low-activity micropattern (i.e., cDMN) in DMN dynamics that

489   was widely distributed in all conscious stages during wakefulness and sleep. In the cDMN, all

490   DMN regions displayed relatively lower levels of activity, implicating that cDMN could be

491   viewed as the silent state for DMN activity in which all the DMN regions preferred relaxations

492   and prepared for the next excitation. However, the cDMN was the only one micropattern

493   during DMN dynamics in which all DMN regions operated in the same manner. Thus, the

494   appearance of the cDMN suggested that there might be a working mode for DMN with low

495   energy, which desired future work to study.

496   **4.2. The balance of dynamic DMN configurations supports consciousness during**

497   **wakefulness.** Based on accumulating evidence, DMN activity is tightly correlated with

498   consciousness levels in health and disease(Buckner et al., 2008; Kapogiannis et al., 2014;

499   Panda et al., 2016; Vanhaudenhuyse et al., 2010). In the AWAKE stage, all the CAMPs showed

500   similar features and the dynamic transitions among them were not statistically different. These

501   similarities illustrated a balanced dynamic configuration among these CAMPs during fast

502   gamma activity in the DMN at rest. The DMN is a key network involved in integrating high-

503   order information from multiple sensory modalities based on numerous projections from

504   variable somatic cortex and core limbic structures (HIP and amygdala) to the DMN

505   regions(Heidbreder and Groenewegen, 2003; Reep et al., 1994). These projections provide the

506   anatomical substrate for the correlation of DMN activity to consciousness levels. Accordingly,

507   the identified balance of DMN dynamics might be a competitive product between the

508   integration and differentiation of CAMPs in maintaining consciousness during wakefulness

509   (Cavanna et al., 2018; Tononi, 2004; Tononi et al., 2016). Furthermore, this balance of

25

510 dynamic configurations also indicated that the DMN might function in multistable regimes

511 and revealed the potential neural mechanism by which DMN activity supports cognitive

512 functions in the resting state(Andrews-Hanna, 2012; Buckner et al., 2008).

513 **4.3. Functional reorganization of the dynamic configurations of the DMN during sleep.**

514 Compared to the resting state, the SWS stage was always accompanied by reduced brain

515 activity, while the commensurate brain activity has been reported in the REM sleep

516 stage(Hobson, 2009; Horovitz et al., 2008). Consistent alterations in the average brain activity

517 associated with CAMPs during DMN dynamics were also observed in our study, suggesting

518 that the activity of CAMPs might also reveal the changes in consciousness during wakefulness

519 and sleep. However, the reduced activity of all CAMPs might not be the main explanation for

520 the decrease in DMN activity observed during deep sleep, due to the stable spatial structures

521 of these CAMPs during wakefulness and sleep. This decrease in activity might result from the

522 increased occurrence probability of the cDMN and the decreased probabilities of the other two

523 high-activity micropatterns. These inversely changed occurrence probabilities in different

524 CAMPs revealed the neural mechanism of reduced activity, that the DMN regions preferred

525 the silent state in deep sleep(Bazhenov et al., 2002; Diekelmann and Born, 2010).

526 The balance of dynamic configurations of the DMN was also disrupted during sleep,

527 indicating the functional reorganization of DMN dynamics. The functional reorganization

528 subsequently led to a loss of consciousness in different sleep stages(Tononi, 2004; Tononi et

529 al., 2016). In the REM sleep stage, the dynamic transitions between aDMN and pDMN

530 increased, indicating more communication between anterior and posterior DMN regions.

531 These communications between anterior and posterior DMN regions might be crucial to

532 primary consciousness, which has been postulated to be preserved in the REM sleep

26

533   stage(Hobson, 2009). Moreover, these communications displayed a combination of both the

534   top-down and bottom-up mechanisms in the DMN. These two mechanisms are important for

535   information processing in the brain(Buschman and Miller, 2007; Theeuwes, 2010), and an

536   enhancement of these mechanisms might help us elucidate the underlying neurophysiological

537   basis for the preservation of primary consciousness during REM sleep.

538   In the SWS stage, the dynamic transitions among CAMPs displayed different changes.

539   The dynamic transitions between the low-activity micropattern and two high-activity

540   micropatterns increased significantly. Additionally, a strong phasic relationship was observed

541   between CAMPs and the up-down states during slow oscillations of the anterior and posterior

542   DMN, and these two types of CAMPs corresponded to different up-down states. Accordingly,

543   the dynamic transitions between the low-activity micropattern and two high-activity

544   micropatterns were deemed to be the transitions within up-down states in the DMN. The

545   dominant transitions of up-down states in deep sleep further provided the physiological

546   importance for these increased dynamic transitions. However, the dynamic transitions within

547   the two high-activity micropatterns decreased in the SWS stage. These reductions supported

548   our hypothesis that communications between anterior and posterior DMN regions are

549   important for primary consciousness, since both higher cognitive functions and primary

550   consciousness are lost during deep sleep (Hobson and Pace-Schott, 2002). The loss of higher

551   cognitive functions might not be caused by the change in a single type of dynamic transitions

552   within pairs of CAMPs. We speculated that the balance of dynamic configurations of the DMN

553   is the underlying neural mechanism supporting higher cognitive functions, which emerged in

554   wakefulness and were deactivated during sleep. The coordination and cooperation of all

555   CAMPs played a core role in the ability of the DMN to perform higher cognitive functions.

556
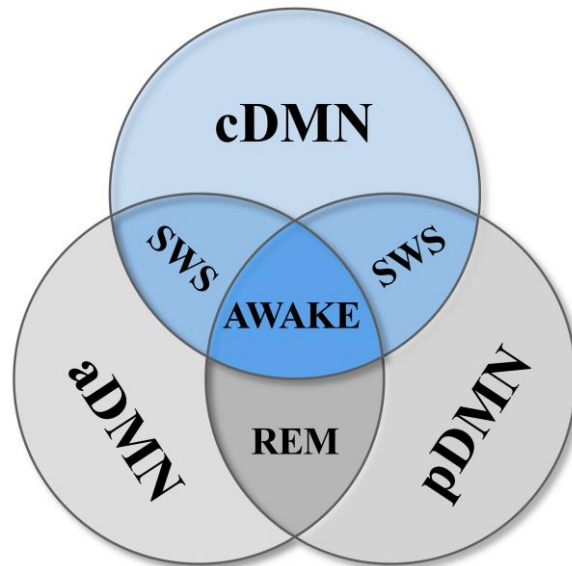
Fig. 6. The three-state model of the consciousness levels during wakefulness and sleep. The AWAKE stage requires the cooperation of all three CAMPs, while the SWS stage requires communications between the low-activity micropattern (cDMN) and the high-activity micropatterns (aDMN or pDMN). The REM sleep stage requires interactions within the two high-activity micropatterns.

Based on these findings, here, we propose a three-state model to describe the relationship between DMN micropatterns and the underlying consciousness levels observed during wakefulness and sleep. As shown in Fig. 6, the three CAMPs involved in DMN dynamics are the basis of this model and their interactions refer to the underlying mechanism regulating the consciousness level observed in distinct stages. Equal communications among the three CAMPs support conscious awareness in the AWAKE stage. The communications between the low-activity micropattern (i.e., cDMN) and each of the high-activity micropatterns (i.e., aDMN or pDMN) are important for the SWS stage characterized by a low level of consciousness. However, during the REM sleep with primary consciousness, communications within high-activity micropatterns are the predominant.

According to the proposed three-state model, we conjecture that preservation of conscious awareness not only requires the information processing between anterior and posterior DMN

28

574   regions, but also need all DMN regions silent and relaxed during this process. Information

575   processing within anterior and posterior DMN regions is mediated by up-down and bottom-

576   up mechanisms and is vital for supporting conscious awareness and primary consciousness. A

577   lack of this process could lead to the loss of consciousness in the SWS stage, and this process

578   alone would result in the consciousness level of REM sleep stage that exists as primary

579   consciousness. This phenomenon highlights the importance of the silent pattern for all DMN

580   regions during the resting state with conscious awareness. However, the roles of the silent

581   pattern in DMN regions and the communications within anterior and posterior DMN regions

582   are unable to be validated by performing some other neurostimulation experiments using the

583   currently available neuroimaging methods. Future studies could validate our model and apply

584   it to the human brain through the application of other neuroimaging measures.

585   **4.4. Methodological Perspectives.** Consistent with the promising microstate analysis of

586   EEG/LFP signals(Michel and Koenig, 2018), the CAMP analysis reported in the present study

587   also assumes that brain activity consists of several distinct instantaneous patterns. The

588   difference is that the CAMP method focuses on the nature of brain activity in different regions

589   and extracts micropatterns from envelope signals. Envelope signals imply temporal alterations

590   in brain power, and their decomposition directly reveals brain rhythm dynamics. In addition,

591   the coactive patterns analyzed in the CAMP method were chosen based on the distribution of

592   extreme values in the envelope signals of brain regions, which differs from the method used

593   in a microstate analysis. Local extreme values in envelope signals represent the instantaneous

594   higher/lower activity of brain regions followed by contrasting changes in activity. Therefore,

595   the derived coactive patterns were considered as the activity patterns leading to an inversion

596   of activity among regions in specific brain networks. Therefore, we postulate that this

597   proposed CAMP method will help researchers extract coactive micropatterns in specific brain

598   networks and reveal additional underlying information about fast brain dynamics.

599   **5. Conclusion**

600   In the current work, we developed a CAMP algorithm to reveal the dynamics of gamma

601   activity in rat DMN during wakefulness and sleep. The fast dynamics of gamma activity in the

602   DMN could be decomposed into three different CAMPs, which showed stable spatial

603   structures across three conscious stages. However, the dynamic configurations of them are

604   specific to different conscious stages. Besides, we also indicated temporal sequence of the

605   neural relationship between up-down states and these CAMPs during deep sleep. Taken

606   together, our results provided functional descriptions for the dynamics of gamma activity in

607   rat DMN during different conscious stage, and proposed a three-state model to reveal the

608   fundamental neural associations between DMN activity with consciousness levels.

609   **CRediT authorship contribution statement**

610   Yan Cui: Methodology, Formal analysis, Visualization, Writing-Original draft preparation,

611   Min Li: Methodology. Bharat Biswal: Investigation, Validation, Writing-Reviewing & Editing.

612   Wei Jing: Data curation, Visualization. Changsong Zhou: Validation, Writing- Reviewing &

613   Editing. Huixiao Liu: Formal analysis. Yang Xia: Conceptualization, Resources. Daqing Guo:

614   Conceptualization, Visualization, Funding acquisition, Writing-Reviewing & Editing.

615   Dezhong Yao: Conceptualization, Project administration, Supervision, Funding acquisition,

616   Writing-Reviewing & Editing.

617   **Declaration of competing interest:** None

618   **Acknowledgements**

References

625   Amzica, F., Steriade, M., 1995. Short- and long-range neuronal synchronization of the slow

626   (<1   Hz)   cortical   oscillation.   J.   Neurophysiol.   73,   20–38.

627   https://doi.org/10.1152/jn.1995.73.1.20

628   Andrews-Hanna, J.R., 2012. The Brain's Default Network and its Adaptive Role in Internal

629   Mentation.   Neuroscientist   18,   251–270.

630   https://doi.org/10.1016/j.neuroimage.2013.08.045

631   Bazhenov, M., Timofeev, I., Steriade, M., Sejnowski, T.J., 2002. Model of thalamocortical

632   slow-wave sleep oscillations and transitions to activated states. J. Neurosci. 22, 1.

633   Beckmann, C.F., DeLuca, M., Devlin, J.T., Smith, S.M., 2005. Investigations into resting-state

634   connectivity using independent component analysis. Philos. Trans. R. Soc. B Biol. Sci.

635   360, 1001–1013. https://doi.org/10.1098/rstb.2005.1634

636   Brett L. Foster, Mohammad Dastjerdi,   and J.P., 2012. Neural populations in human

637   posteromedial cortex display opposing responses during memory and numerical

638   processing.   Proc.   Natl.   Acad.   Sci.   109,   15514–15519.

639   https://doi.org/10.1073/pnas.1206580109/-

640   /DCSupplemental.www.pnas.org/cgi/doi/10.1073/pnas.1206580109

641   Buckner, R.L., Andrews-Hanna, J.R., Schacter, D.L., 2008. The brain's default network:

642   Anatomy, function, and relevance to disease. Ann. N. Y. Acad. Sci. 1124, 1–38.

643   https://doi.org/10.1196/annals.1440.011

644   Buschman, T.J., Miller, E.K., 2007. Top-Down Versus Bottom-Up Control of Attention in the

645   Prefrontal and. Science (80-.). 315, 1860–1863. https://doi.org/10.1126/science.1138071

646   Cavanna, F., Vilas, M.G., Palmucci, M., Tagliazucchi, E., 2018. Dynamic functional

647   connectivity and brain metastability during altered states of consciousness. Neuroimage

648   180, 383–395. https://doi.org/10.1016/j.neuroimage.2017.09.065

649   Cui, Y., Yu, S., Zhang, T., Zhang, Y., Xia, Y., Yao, D., Guo, D., 2018. Altered activity and

650   information flow in the default mode network of pilocarpine-induced epilepsy rats. Brain

651   Res. 1696, 71–80. https://doi.org/10.1016/j.brainres.2018.05.012

652   Diekelmann, S., Born, J., 2010. The memory function of sleep. Nat. Rev. Neurosci. 11, 114–

653   26. https://doi.org/10.1038/nrn2762

654   Foster, B.L., Rangarajan, V., Shirer, W.R., Parvizi, J., 2015. Intrinsic and task-dependent

655   coupling of neuronal population activity in human parietal cortex. Neuron 86, 578–590.

656   https://doi.org/10.1016/j.neuron.2015.03.018

657   Fox, K.C.R., Foster, B.L., Kucyi, A., Daitch, A.L., Parvizi, J., 2018. Intracranial

658   Electrophysiology of the Human Default Network. Trends Cogn. Sci.

659   https://doi.org/10.1016/j.tics.2018.02.002

660   Fox, M.D., Snyder, A.Z., Vincent, J.L., Corbetta, M., Essen, C. Van, Raichle, M.E., Fox, M.D.,

661   Snyder, A.Z., Vincent, J.L., Corbetta, M., Essen, D.C. Van, Raichle, M.E., 2016.

662   Networks Linked references are available on JSTOR for this article : The human brain is

663   intrinsically organized into dynamic , anticorrelated functional networks. Proc. Natl.

664   Acad. Sci. U. S. A.

665   Gusnard, D.A., Akbudak, E., Shulman, G.L., Raichle, M.E., 2001. Medial prefrontal cortex

666   and self-referential mental activity: Relation to a default mode of brain function. Proc.

667   Natl. Acad. Sci. U. S. A. 98, 4259–4264. https://doi.org/10.1073/pnas.071043098

668   Hagmann, P., Cammoun, L., Gigandet, X., Meuli, R., Honey, C.J., Van Wedeen, J., Sporns, O.,

669   2008. Mapping the structural core of human cerebral cortex. PLoS Biol. 6, 1479–1493.

670   https://doi.org/10.1371/journal.pbio.0060159

671   Heidbreder, C.A., Groenewegen, H.J., 2003. The medial prefrontal cortex in the rat: Evidence

672   for a dorso-ventral distinction based upon functional and anatomical characteristics.

673   Neurosci. Biobehav. Rev. 27, 555–579. https://doi.org/10.1016/j.neubiorev.2003.09.003

674   Hobson, J.A., 2009. REM sleep and dreaming: Towards a theory of protoconsciousness. Nat.

675   Rev. Neurosci. 10, 803–814. https://doi.org/10.1038/nrn2716

676   Hobson, J.A., Pace-Schott, E.F., 2002. The cognitive neuroscience of sleep: Neuronal systems,

677   consciousness   and   learning.   Nat.   Rev.   Neurosci.   3,   679–693.

678   https://doi.org/10.1038/nrn915

679   Holcman, D., Tsodyks, M., 2006. The emergence of up and down states in cortical networks.

680   PLoS Comput. Biol. 2, 174–181. https://doi.org/10.1371/journal.pcbi.0020023

681   Horovitz, S.G., Fukunaga, M., De Zwart, J.A., Van Gelderen, P., Fulton, S.C., Balkin, T.J.,

682   Duyn, J.H., 2008. Low frequency BOLD fluctuations during resting wakefulness and

683   light sleep: A simultaneous EEG-fMRI study. Hum. Brain Mapp. 29, 671–682.

684   https://doi.org/10.1002/hbm.20428

685   Ji, D., Wilson, M.A., 2007. Coordinated memory replay in the visual cortex and hippocampus

686   during sleep. Nat. Neurosci. 10, 100–107. https://doi.org/10.1038/nn1825

687   Jing, W., Guo, D., Zhang, Y., Guo, F., Valdés-Sosa, P.A., Xia, Y., Yao, D., 2017. Reentrant

688   information flow in electrophysiological rat default mode network. Front. Neurosci. 11,

689   1–12. https://doi.org/10.3389/fnins.2017.00093

690   Kapogiannis, D., Reiter, D.A., Willette, A.A., Mattson, M.P., 2014. Dynamic functional

691   connectivity of the default mode network tracks daydreaming. Neuroimage 100, 112–119.

692   https://doi.org/10.1016/j.neuroimage.2012.09.029.Posteromedial

693   Karim Jerbi*†, R., V.J., Tomas, , O., Dalal, S.S., Julien Jung, D.H., Minotti, L., Bertrand1,

694   O., Kahane, P., Lachaux, and J.-P., 2010. Exploring the electrophysiological correlates

695   of the default-mode network with intracerebral EEG. Front. Syst. Neurosci. 4, 1–9.

696   https://doi.org/10.3389/fnsys.2010.00027

697   Larson-Prior, L.J., Zempel, J.M., Nolan, T.S., Prior, F.W., Snyder, A., Raichle, M.E., 2009.

698   Cortical network functional connectivity in the descent to sleep. Proc. Natl. Acad. Sci. U.

699   S. A. 106, 4489–4494. https://doi.org/10.1073/pnas.0900924106

700   Lehmann, D., Faber, P.L., Galderisi, S., Herrmann, W.M., Kinoshita, T., Koukkou, M., Mucci,

701   A., Pascual-Marqui, R.D., Saito, N., Wackermann, J., Winterer, G., Koenig, T., 2005.

702   EEG microstate duration and syntax in acute, medication-naïve, first-episode

703   schizophrenia: A multi-center study. Psychiatry Res. - Neuroimaging 138, 141–156.

704   https://doi.org/10.1016/j.pscychresns.2004.05.007

705   Liu, Q., Farahibozorg, S., Porcaro, C., Wenderoth, N., Mantini, D., 2017. Detecting large-scale

706   networks in the human brain using high-density electroencephalography. Hum. Brain

707   Mapp. 38, 4631–4643. https://doi.org/10.1002/hbm.23688

708 Liu, X., Chang, C., Duyn, J.H., 2013. Decomposition of spontaneous brain activity into
709   distinct fMRI co-activation patterns. Front. Syst. Neurosci. 7, 1–11.
710   https://doi.org/10.3389/fnsys.2013.00101

711 Liu, X., Duyn, J.H., 2013. Time-varying functional network information extracted from brief
712   instances of spontaneous brain activity. Proc. Natl. Acad. Sci. U. S. A. 110, 4392–7.
713   https://doi.org/10.1073/pnas.1216856110

714 Logothetis, N.K., 2002. The neural basis of the blood-oxygen-level-dependent functional
715   magnetic resonance imaging signal. Philos. Trans. R. Soc. B Biol. Sci. 357, 1003–1037.
716   https://doi.org/10.1098/rstb.2002.1114

717 Logothetis, N.K., Pauls, J., Augath, M., Trinath, T., Oeltermann, A., 2001. Neurophysiological
718   investigation of the basis of the fMRI signal. Nature 412, 150–157.
719   https://doi.org/10.1038/35084005

720 Lőrincz, M.L., Gunner, D., Bao, Y., Connelly, W.M., Isaac, J.T.R., Hughes, S.W., Crunelli, V.,
721   2015. A distinct class of slow (~0.2–2 Hz) intrinsically bursting layer 5 pyramidal neurons
722   determines UP/DOWN state dynamics in the neocortex. J. Neurosci. 35, 5442–5458.
723   https://doi.org/10.1523/JNEUROSCI.3603-14.2015

724 Lu, H., Zou, Q., Gu, H., Raichle, M.E., Stein, E.A., Yang, Y., 2012. Rat brains also have a
725   default mode network. Proc. Natl. Acad. Sci. U. S. A. 109, 3979–84.
726   https://doi.org/10.1073/pnas.1200506109

727 Magri, C., Schridde, U., Murayama, Y., Panzeri, S., Logothetis, N.K., 2012. The Amplitude
728   and Timing of the BOLD Signal Reflects the Relationship between Local Field Potential
729   Power at Different Frequencies. J. Neurosci. 32, 1395–1407.
730   https://doi.org/10.1523/JNEUROSCI.3985-11.2012

731 Michel, C.M., Koenig, T., 2018. EEG microstates as a tool for studying the temporal dynamics
732   of whole-brain neuronal networks: A review. Neuroimage 180, 577–593.
733   https://doi.org/10.1016/j.neuroimage.2017.11.062

734 Ongur, D., Price, J., 2000. The Organization of Networks within the Orbital and Medial
735   Prefrontal Cortex of Rats, Monkeys and Humans. Cereb. Cortex 10, 206–219.
736   https://doi.org/10.1093/cercor/10.3.206

737 Ossandon, T., Jerbi, K., Vidal, J.R., Bayle, D.J., Henaff, M.-A., Jung, J., Minotti, L., Bertrand,

738   O., Kahane, P., Lachaux, J.-P., 2011. Transient Suppression of Broadband Gamma Power
739   in the Default-Mode Network Is Correlated with Task Complexity and Subject
740   Performance. J. Neurosci. 31, 14521–14530. https://doi.org/10.1523/JNEUROSCI.2483-
741   11.2011

742   Panda, R., Bharath, R.D., Upadhyay, N., Mangalore, S., Chennu, S., Rao, S.L., 2016. Temporal
743   Dynamics of the Default Mode Network Characterize Meditation-Induced Alterations in
744   Consciousness. Front. Hum. Neurosci. 10, 1–12.
745   https://doi.org/10.3389/fnhum.2016.00372

746   Petersen, C.C.H., Hahn, T.T.G., Mehta, M., Grinvald, A., Sakmann, B., 2003. Interaction of
747   sensory responses with spontaneous depolarization in layer 2/3 barrel cortex. Proc. Natl.
748   Acad. Sci. U. S. A. 100, 13638–13643. https://doi.org/10.1073/pnas.2235811100

749   Raichle, M.E., 2015. The Brain ' s Default Mode Network. Annu. Rev. Neurosci. 413–427.
750   https://doi.org/10.1146/annurev-neuro-071013-014030

751   Raichle, M.E., MacLeod, A.M., Snyder, A.Z., Powers, W.J., Gusnard, D.A., Shulman, G.L.,
752   2001. A default mode of brain function. Proc. Natl. Acad. Sci. U. S. A. 98, 676–82.
753   https://doi.org/10.1073/pnas.98.2.676

754   Raichle, M.E., Mintun, M.A., 2006. Brain work and brain imaging. Annu. Rev. Neurosci. 29,
755   449–76. https://doi.org/10.1146/annurev.neuro.29.051605.112819

756   Reep, R.L., Chandler, H.C., King, V., Corwin, J. V., 1994. Rat posterior parietal cortex:
757   topography of corticocortical and thalamic connections. Exp. Brain Res. 100, 67–84.
758   https://doi.org/10.1007/BF00227280

759   Rosazza, C., Minati, L., 2011. Resting-state brain networks: Literature review and clinical
760   applications. Neurol. Sci. 32, 773–785. https://doi.org/10.1007/s10072-011-0636-y

761   Sämann, P.G., Wehrle, R., Hoehn, D., Spoormaker, V.I., Peters, H., Tully, C., Holsboer, F.,
762   Czisch, M., 2011. Development of the brain's default mode network from wakefulness
763   to slow wave sleep. Cereb. Cortex 21, 2082–2093. https://doi.org/10.1093/cercor/bhq295

764   Scheering, R., Koopmans, P.J., Van Mourik, T., Jensen, O., Norris, D.G., 2016. The
765   relationship between oscillatory EEG activity and the laminar-specific BOLD signal.
766   Proc. Natl. Acad. Sci. U. S. A. 113, 6761–6766. https://doi.org/10.1073/pnas.1522577113

767   Theeuwes, J., 2010. Top-down and bottom-up control of visual selection. Acta Psychol.

768   (Amst). 135, 77–99. https://doi.org/10.1016/j.actpsy.2010.02.006

769   Tononi, G., 2004. An information integration theory of consciousness., BMC neuroscience.

770   BioMed Central. https://doi.org/10.1186/1471-2202-5-42

771   Tononi, G., Boly, M., Massimini, M., Koch, C., 2016. Integrated information theory: From

772   consciousness to its physical substrate. Nat. Rev. Neurosci.

773   https://doi.org/10.1038/nrn.2016.44

774   Vanhaudenhuyse, A., Noirhomme, Q., Tshibanda, L.J.F., Bruno, M.A., Boveroux, P.,

775   Schnakers, C., Soddu, A., Perlbarg, V., Ledoux, D., Brichant, J.F., Moonen, G., Maquet,

776   P., Greicius, M.D., Laureys, S., Boly, M., 2010. Default network connectivity reflects the

777   level of consciousness in non-communicative brain-damaged patients. Brain 133, 161–

778   171. https://doi.org/10.1093/brain/awp313

779   Vidaurre, D., Smith, S.M., Woolrich, M.W., 2017. Brain network dynamics are hierarchically

780   organized in time. Proc. Natl. Acad. Sci. 201705120.

781   https://doi.org/10.1073/pnas.1705120114

782   Wu, X. jie, Zeng, L.L., Shen, H., Yuan, L., Qin, J., Zhang, P., Hu, D., 2017. Functional network

783   connectivity alterations in schizophrenia and depression. Psychiatry Res. - Neuroimaging

784   263, 113–120. https://doi.org/10.1016/j.pscychresns.2017.03.012

785   Wyss, J.M., Vangroen, T., 1992. Connections between the retrosplenial cortex and the

786   hippocampal-formation in the rat - a review. Hippocampus 2, 1–12.

787   https://doi.org/10.1002/hipo.450020102

788